MethodsX 13 (2024) 103036

Contents lists available at ScienceDirect

MethodsX

journal homepage: www.elsevier.com/locate/methodsx

Quantification of bacterial shape using moment invariants enables distinguishing populations during cellular plasmolysis ☆,☆☆

Braulio Gutiérrez–Medina

Division of Advanced Materials, Instituto Potosino de Investigación Científica y Tecnológica, Camino a la Presa San José 2055, San Luis Potosí 78216, Mexico

ARTICLE INFO

Method name:
Quantitative analysis of bacterial shape

Keywords:
Cell shape
Bacterial plasmolysis
Moment invariants
Cell contour

ABSTRACT

The analysis of geometrical cell shape is fundamental to understand motility, development, and responses to external stimuli. The moment invariants framework quantifies cellular shape and size, although its applicability has not been explored for rod-shaped bacteria. In this work, we use moment invariants to evaluate the extent of cell shape change (projected area and volume) during plasmolysis, as *Escherichia coli* cells are subjected to hyperosmotic shock. The characteristic cell size descriptors width, length and area show systematic decrease as external salt (NaCl) conditions increase—except for high salt, where a small population of cells shows evidence of membrane rupture. We use these two-dimensional results to estimate cell volume during plasmolysis, finding a minimum volume that is not reduced further with increase in salt concentration. Next, we computed elongation and dispersion, metrics that quantify how cell shape is stretched out or differs from an ellipse, respectively. For dispersion, we observe the development of a long tail for the distribution at high salt. Moreover, the use of elongation-dispersion plots enables distinction of plasmolyzed and normal cells despite the presence of broad distributions. Altogether, a protocol is provided to evaluate bacterial shape, highlighting a set of metrics that help distinguish among bacterial populations.

- Moment invariants enable quantitative description of bacterial morphology in two dimensions, and estimation of volume
- We apply the moment invariants framework to describe changes in bacterial shape during plasmolysis
- The proposed methodology shows suitability to distinguish among cellular populations.

☆ **Related research article:** Experimental data was drawn from: B. Gutiérrez-Medina and M. de J. Sánchez Miranda, "Quantitative Image Restoration in Bright Field Optical Microscopy," Biophys J, vol. 113, no. 9, pp. 1916–1919, Nov. 2017, doi: 10.1016/j.bpj.2017.09.002.

☆☆ **For a published article:** Experimental data was drawn from: B. Gutiérrez-Medina and M. de J. Sánchez Miranda, "Quantitative Image Restoration in Bright Field Optical Microscopy," Biophys J, vol. 113, no. 9, pp. 1916–1919, Nov. 2017, doi: 10.1016/j.bpj.2017.09.002.

E-mail address: bgutierrez@ipicyt.edu.mx

https://doi.org/10.1016/j.mex.2024.103036
Received 15 July 2024; Accepted 4 November 2024
Available online 6 November 2024

Specifications Table

Subject area:	Agricultural and Biological Sciences
More specific subject area:	Microbiology
Name of your method:	Quantitative analysis of bacterial shape
Name and reference of original method:	Moment Invariants G. A. Dunn and A. F. Brown, "Quantifying Cellular Shape Using Moment Invariants," in *Biological Motion: Proceedings of a Workshop held in Königswinter, Germany, March 16–19, 1989*, W. Alt and G. Hoffmann, Eds., Berlin, Heidelberg: Springer Berlin Heidelberg, 1990, pp. 10–34. doi: 10.1007/978-3-642-51664-1_2.
Resource availability:	Any modern PC or laptop

Background

The analysis of geometrical shape is a fundamental step towards understanding cellular motility [1,2], development [3], and response to external stimuli [4,5]. In both prokaryotic and eukaryotic cells, shape arises from the collective formed by several molecular determinants (most notably the cytoskeleton, the cell membrane, among others) in interaction with the physical environment outside of the cell (the extracellular matrix, the substrate). Therefore, analyses of cellular geometry could yield important information about the mechanisms behind how cells translocate, divide, or communicate. Consequently, approaches to inspect cellular geometry have been developed, ranging from optical [6] to electrical methods [7].

A classic pipeline to analyze cellular shape includes image acquisition using optical microscopy, single-cell segmentation, and evaluation of morphology [6,8–12]. In this approach, segmentation enables recovery of the set of (x,y) coordinate points corresponding to the cell boundaries, from where the metrics that characterize cell shape are determined. Typically, specific tagging of the cellular membrane and fluorescence microscopy visualization enables extraction of the cell boundaries, although photobleaching and phototoxicity (for living specimens) are of concern. One attractive alternative to fluorescence microscopy is label-free bright-field microscopy [8]. Indeed, researchers have analyzed Differential Interference Contrast (DIC) microscopy images to extract cell shape, using from edge detection filters [13] to deep learning [14]. In our group, we have previously used plain bright-field imaging and image deconvolution to register bacterial cell shape changes under osmotic pressure [15].

One aspect of cellular morphology that is often evaluated is size, either in terms of area, length or width. Assessment of cellular size is of importance in cytometry or whenever distinct cell populations must be identified; however, several additional shape parameters can be explored (e.g. circularity, elongation, contour concavity, tangent orientations, lobe or branch characteristics, etc.) [16], with the potential to provide useful information towards detailed, robust cell classification schemes. In the effort to quantify cellular shape beyond size, the geometrical moment invariants framework [17] is ideally suited, as it provides a systematic approach that (at least for the first moments) offers a physical interpretation of parameters. Although successfully applied to mammalian cells (well known for their intricated shapes), the invariant moments framework has not been tested for bacteria (where size descriptors are often limited to length, width, and area).

In this work, we use moment invariants to evaluate changes in morphology as *Escherichia coli* cells are subjected to hyperosmotic shock. We find that the parameters derived from the geometrical moments are useful to characterize the deformation of the bacterial cells during plasmolysis. Furthermore, assuming symmetry in the rod-shaped bacteria and using a scaling argument, we show it is possible to estimate cellular volume. Our work demonstrates a tool to evaluate cellular size metrics beside area, contributing to available protocols aimed at sizing bacteria, providing metrics that help distinguish between bacterial populations.

Method details

Sample preparations, imaging, and extraction of cell contour. The following procedures have been fully described in Ref. [15].

- Sample preparations and imaging. *E. coli* BL21 DE3 cells were cultured overnight in Luria Broth (LB) at 37 ˚C under constant shaking and used for fluorescence staining. For hyperosmotic shock, bacteria were subcultured to reach an optical density of ∼0.6–0.8 and used for experiments. To induce hyperosmotic conditions, a sample of cells was introduced in microscopy flow chambers and left to bind to poly-L-lysine-coated coverslips for 15 min. LB was exchanged with 10 mM Tris–HCl (pH 7.5), and buffer exchange was performed with the Tris–HCl buffer supplemented with NaCl at one of the following concentrations: 0 M, 0.25 M, 0.5 M, and 1.0 M Finally, the flow cell was then sealed using valap, and samples were taken to the microscope for observation.
- To perform bright-field imaging, a home-made microscope was set to Kohler illumination, with the numerical aperture of the condenser adjusted to 0.1. The microscope included: a light emitting diode (LED) with peak wavelength λ∼450 nm as the illumination source, a 100 × detection objective lens (oil immersion, NA = 1.3, Olympus), a z-axis piezoelectric stage (Nano-Z200, Mad City Labs, Madison, WI), and an 8-bit charge-coupled device (CCD) camera (MV-D1024E-160-CL, Photonfocus, Lachen, Switzerland). These steps were followed: (i) the microscope was first set in focus and then defocused using the automated z-stage to the pre-established value $z = -2$ µm. $z < 0$ values correspond to the objective lens moving away from the specimen; (ii) 30 frames were acquired and averaged, providing a single image that was transferred to a computer for off-line digital processing; (iii) the microscope stage was moved to sample a different field of view, then repeating steps (i)-(ii).
- To implement quantitative image restoration in bright field (QRBF) [15], 2D deconvolution was performed on single BF images of bacteria attached to coverslips, using an iterative deconvolution algorithm available in the ImageJ plugin Deconvolution

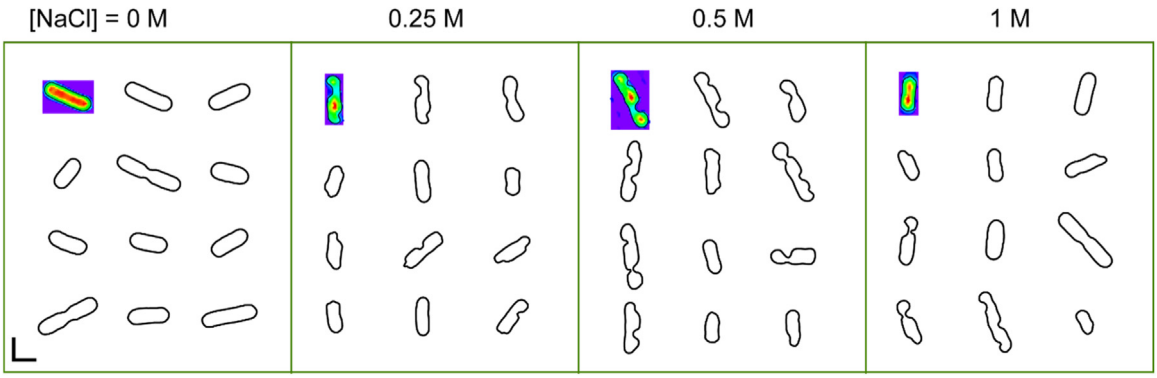

Fig. 1. Typical examples of cell contours for increasing salt concentration. False-color insets show final cell images after deconvolution, whereas extracted cell contours are shown as black lines. Scale bar: 1 μm.

Lab [15,18]. The PSF used to perform deconvolution was generated by first computing a 3D theory-based PSF, and then by extracting the single *x-y* slice that has the same amount of defocus as the experimental images ($z = -2$ μm). Parameters used in Deconvolution Lab: *Algorithm* = Tikhonov-Miller; *regularization parameter (lambda)* = 0.005; *number of iterations (k)* = 100; *positivity constraint* = true; *normalize PSF* = true; *recenter PSF* = true; *initial estimation* = *a* blank image; *use FFTW* = false. No further processing for image appearance was performed after deconvolution.

- Cell image segmentation. The following digital processes were carried out in ImageJ on deconvolved images. 1) Median smoothing (radius=1); 2) Threshold, leaving unmodified pixels with counts above the value 13.0, and setting counts of all other pixels to zero; 3) Binarize; 4) *Analyze Particles*, with parameters (*size*=180–600 pixels^2, *circularity*=0.0–0.8, *show*=Masks); 5) Dilate identified particles; 6) *Analyze Particles*, with parameters (*size*=0-Infinity pixels^2, *circularity*=0.0–1.0), recording the bounding box coordinates of each particle found; and 7) Use bounding box coordinates to duplicate images of individual bacteria, and store images for posterior analysis.
- Bacterial cell contour. We applied the following procedure for each image of individual bacteria. 1) The average pixel intensity (I_{avg}) was found, for those pixels with count values above 10 (to avoid including background). 2) A threshold value (I_{th}) was established: $I_{th} = T \times I_{avg}$, with $T = 0.6$. 3) The cellular contour is the collection of points with intensity values corresponding to I_{th}. To find these points, (*i,j*) pixels with intensity value $I_{i,j} > I_{th}$ were first identified, and then the eight neighbor pixels were further analyzed. When a (*k,l*) neighbor pixel with intensity $I_{k,l} < I_{th}$ was found, the coordinates (x_n,y_n) of the *n*-th cell contour point was produced by linear interpolation between the (*i,j*) and (*k,l*) pixels: $x_n = f \times (I_{i,j} - I_{th})/(I_{i,j} - I_{k,l}) + i$, where *f* can take the values (0, 1, $\sqrt{2}$) depending on the location of the (*k,l*) pixel with respect to the (*i,j*) pixel (above or below, left or right, diagonal, respectively). The corresponding procedure was followed to find y_n. Typically, each bacterium contour consisted of $N \sim 200$ points. Finally, points were sorted based on Euclidean distance, a 5-point binomial overall smoothing was applied, and the coordinates of the endpoints were made equal by averaging. Cell contour analysis was performed using Igor Pro.

The moment invariants method, and its application to bacterial cells under hyperosmotic shock

We previously obtained the contours of *E. coli* cells subjected to increasing concentrations of NaCl using two-dimensional quantitative image restoration in bright field (2D-QRBF) [15]. In 2D-QRBF, immobilized cells were imaged using high-contrast bright-field optical microscopy under a slight (2 μm) defocus, recorded images were deconvolved with a (phase) point spread function with the same defocus, and subsequent segmentation enabled extraction of the set of coordinates $C_k = \{(x,y)\}_k$ corresponding to the contour of the *k*th cell. The set of contour coordinates C constitutes the starting point for the analysis performed in the present work.

Fig. 1 shows how the initial rod-shape typical of bacteria under no external stress ([NaCl] = 0) changes as salt concentration increases. Under the influence of hyperosmotic stress, bacteria develop plasmolysis, where plasma membrane contraction limits the extent of the cytoplasm. This effect causes bacteria to change shape under the optical microscope. Our images (Fig. 1) show the development of invaginations and contractions in cells that increase in number and extent as salt concentration increases. Despite this behavior, we find that for [NaCl] = 1 M some bacteria show an apparent normal shape (no deformations), suggesting rupture of the plasma cell membrane and filling by the cytoplasm of the capsule defined by the cell wall.

To characterize changes in cellular morphology during plasmolysis, we use the two-dimensional geometrical moment invariants [17]. The raw moments are given by:

$$m_{jk} = \int_{-\infty}^{\infty}\int x^j y^k f(x,y)\mathrm{d}x\mathrm{d}y$$

where *j* and *k* are non-negative integer numbers, the order of each moment is $j + k$, and the function $f(x,y)$ represents mass distribution. We assume $f(x,y) = 1$ for points located within the cell body and 0 elsewhere, as our aim is to provide a geometrical description of

cells. For digitized cell images, and provided the set of n coordinate pairs C = {(x,y)} for a given cell outline, the raw moments can be calculated as [17]:

$$a_i = 0.5\left(x_i y_{i-1} - x_{i-1} y_i\right)$$

$$m_{00} = \sum_{i=1}^{n} a_i \tag{1}$$

$$m_{10} = \frac{1}{3}\sum_{i=1}^{n} a_i\left(x_{i-1} + x_i\right) \tag{2}$$

$$m_{20} = \frac{1}{6}\sum_{i=1}^{n} a_i\left(x_{i-1}^2 + x_{i-1}x_i + x_i^2\right) \tag{3}$$

$$m_{11} = \frac{1}{12}\sum_{i=1}^{n} a_i\left(2x_{i-1}y_{i-1} + x_{i-1}y_i + x_i y_{i-1} + 2x_i y_i\right) \tag{4}$$

with corresponding formulas for m_{01} and m_{02}. These values depend on the cell area. To obtain values for the moments that are invariant to translation, dilation and rotation, the moment invariants are calculated [17]. Starting from the raw moments, the central moments ($'m_{jk}$) are first obtained:

$$'m_{20} = m_{20} - a\bar{x}^2 \tag{5}$$

$$'m_{11} = m_{11} - a\bar{x}\bar{y} \tag{6}$$

$$'m_{02} = m_{02} - a\bar{y}^2 \tag{7}$$

$$\bar{x} = \frac{m_{10}}{m_{00}}; \bar{y} = \frac{m_{01}}{m_{00}}$$

and are invariant to translation. Here, $a = m_{00}$ is cell area, and ($\bar{x}$, $\bar{y}$) centroid coordinates. Next, invariance to change of scale is achieved with the normalized central moments:

$$''m_{jk} = '\,m_{jk}/a^{(j+k+2)/2} \tag{8}$$

Finally, the rotational invariants ($'''m_{jk}$) are obtained as:

$$'''m_{20} = ''\,m_{20}c^2 + 2''m_{11}cs + ''\,m_{02}s^2 \tag{9}$$

$$'''m_{02} = ''\,m_{20}s^2 - 2''m_{11}cs + ''\,m_{02}c^2 \tag{10}$$

$$\varphi = \frac{1}{2}\tan^{-1}\left[\frac{2''m_{11}}{''m_{20} - ''\,m_{02}}\right];\ c = \cos(\varphi);\ s = \sin(\varphi)$$

These metrics (Eq. (9)-10) are called the moment invariants, and are descriptors of shape independent of scale, choice of coordinate axes (location and orientation).

Method validation

To apply this framework to bacteria under hyperosmotic shock, we start by computing characteristic cell length and width and comparing with previously published results. We recall the concept of the equimomental ellipse, where it is possible to find a unique elliptical shape with the same invariant moments corresponding to the original shape through the second order [17,19]. The long and short radii of the equimomental ellipse are given by:

$$A = 2\sqrt{'''m_{20}}\ and\ B = 2\sqrt{'''m_{02}} \tag{11}$$

respectively. Fig. 2 shows the computed cell length $L = 2A\sqrt{m_{00}}$, and width $W = 2B\sqrt{m_{00}}$ for the bacterial cell populations subject to increasing salt concentration.

At [NaCl] = 0, the distribution for length is broader compared with width, reflecting the fact that cells are imaged during various stages of cell duplication. Upon hyperosmotic shock, bacteria undergo compaction in size, where the mean of the distributions for both length and width decrease linearly with increased salt concentration until [NaCl] = 0.5 M (see insets in Fig. 2B). At [NaCl] = 1 M cell size is not reduced further; in addition, a small population emerges with increased width and length (see Fig. 2A), thus confirming the qualitative observation that at the highest salt concentration some cells show a shape similar to the no salt condition.

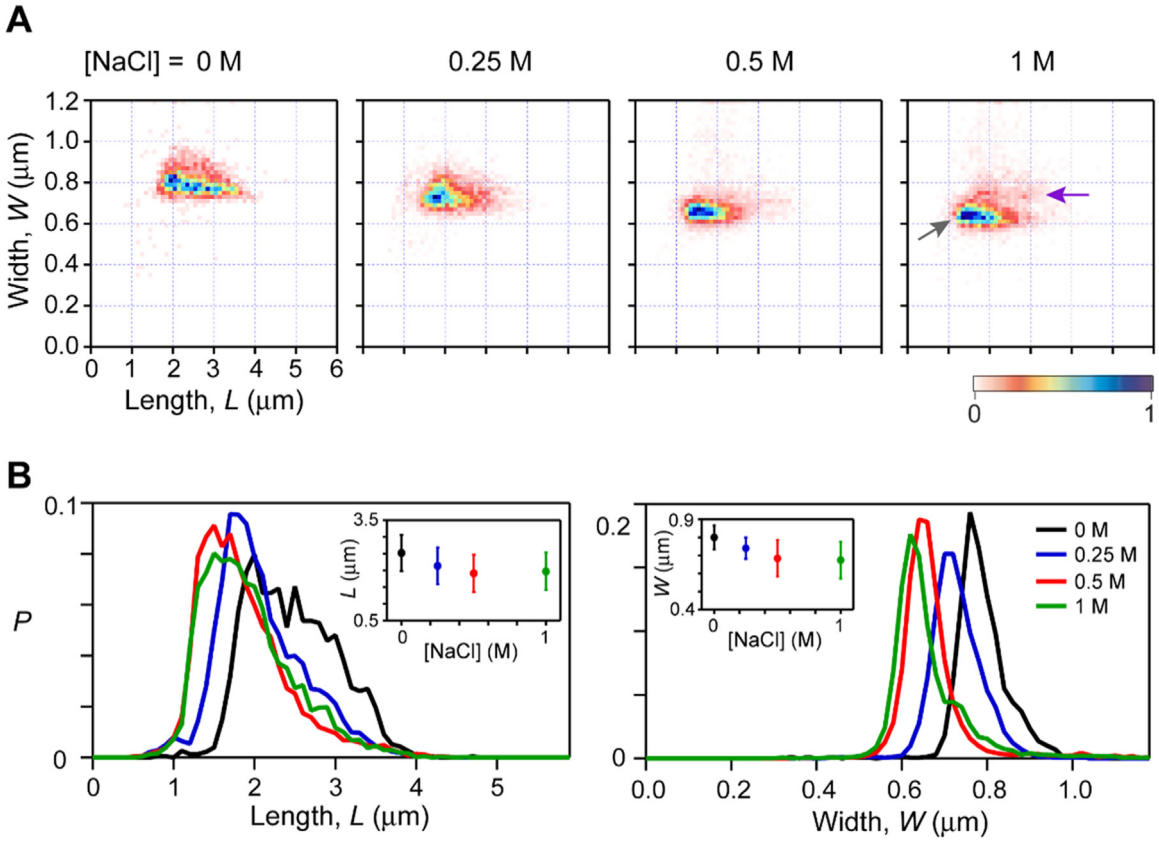

Fig. 2. Characteristic cell length and width during hyperosmotic shock, computed using the invariant moments approach. (A) 2D histograms of length vs. width. At [NaCl] = 1 M a small population emerges (violet arrow), distinct from the main population (gray arrow). (B) Normalized distribution of length (left) and width (right) for various salt concentrations. Insets show mean and standard deviation (error bars) values of the distributions. N = 2337 (0 M), 4654 (0.25 M), 6801 (0.5 M), 6150 (1 M).

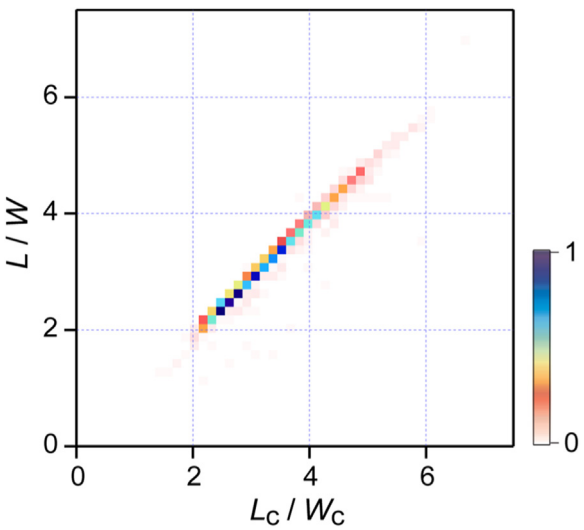

Fig. 3. Comparison of the ratio length/width obtained using two independent methods. The values L/W are computed using the invariant moments, whereas the values L_c/W_c (L_c, W_c represent "caliper" length and width, respectively) are computed using measurements of cell length and width at various positions within the cell body (see Ref. [15]).

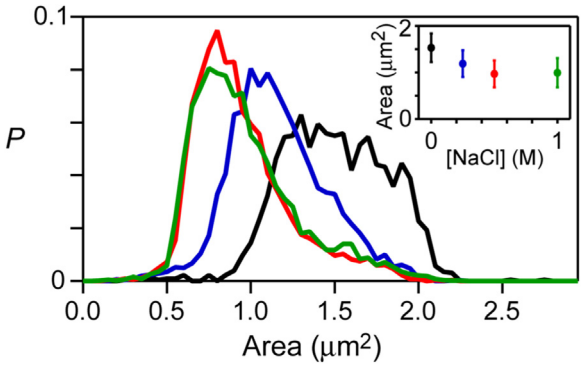

Fig. 4. Behavior of cell area distribution upon increase in NaCl concentration. Inset shows mean values; error bars: SD.

The results for characteristic length and width using the invariant moments (Fig. 2) are comparable to a previously published result (Fig. 2B-C in Ref. [15]) that used a much more involved "caliper" method (based on the assumption that the cell has one main axis, and on averaging measurements of width at various positions within the cell body). A plot of the ratio length/width for the two methods is shown in Fig. 3, revealing identity between the two approaches. From these observations, we conclude that the invariant moments method yields accurate results for characteristic cell length and width, with the advantage of simplicity and that no assumptions are needed. Moreover, the geometrical moments provide further information about the shape of the cell (as shown below).

Next, we consider the behavior of cell area (m_{00}) as a function of salt concentration (Fig. 4). At [NaCl] = 0, we observe a broad distribution (corresponding to cells caught in various phases of development) with mean ~1.5 μm^2. Cell area decreases with salt increase, and the corresponding distributions for [NaCl] = 0.5 M and 1.0 M are similar, with mean cell area ~1.0 μm^2. The distributions at the highest salt concentrations also reveal that cell area does not reach below $A_{\min}$ ~0.6 μm^2. These results can be used to estimate cell volume, using the symmetry present in rod-shaped bacteria and scaling. We asked what fraction of the original cell volume this lower area limit represents. At [NaCl] = 0 M we consider the bacterial cell as a cylinder of length l_0 capped by two hemispheres of radii r; the cell volume is $V_0 = \pi r^2 l_0 + (4/3)\pi r^3$ and the projected area is $A_0 = 2rl_0 + \pi r^2$. In this last formula, we take A_0 = 1.5 μm^2 and r = 0.4 μm (at [NaCl] = 0 we measured a mean cell width ~0.8 μm), from where l_0 = 1.25 μm. Substituting the values for r and l_0 in the expression for cell volume, we find V_0 = 0.9 μm^3. Now, for $A_{\min}$ at [NaCl] = 0.5 M, the cell has shrunk considerably and therefore we approximate $V_{\min} = (A_{\min})^{3/2}$ = 0.46 μm^3 = 0.5V_0. Therefore, we conclude that at [NaCl] = 0.5 M the minimum volume enclosed by the cell membrane is about half of the original cell volume. Moreover, this minimum volume does not decrease upon increase of salt concentration beyond 0.5 M

The invariant moments framework offers two additional metrics that characterize cellular geometry regardless of scale, orientation or position: elongation and dispersion. The characteristic elongation (E) of the cell can be evaluated using the long (A) and short (B) radii of the equimomental ellipse (see Eq. (11)) as: $E = \log_2 (A/B)$. Elongation is zero when the cell is not elongated (a circle) and one if A/B = 2. We computed elongation values for bacterial cells under increasing salt conditions (Fig. 5A, left). The distributions are wide, and shift towards lower values as salt concentration increases. At [NaCl] = 0 nearly all cells have elongation values above 1.0, with $E_{0\ M} = 1.63 \pm 0.34$, whereas at [NaCl] = 0.5 M about 17 % of cells show elongation values below 1.0, and $E_{0.5\ M} = 1.44 \pm 0.40$ (mean ± SD). Correspondingly, the equimomental ellipse has values A/B = 3.1 ([NaCl] = 0) and A/B = 2.7 ([NaCl] = 0.5 M). These observations are consistent with the notion that plasmolyzed cells adopt a more compact geometry compared to the unperturbed elongated shape and provide a quantitative distinction between the two populations. Yet, even at high salt concentration cells show significant elongation.

Dispersion characterizes how much the shape of the cell compares with an ellipse [17], and it is calculated as $D = \log_2(\pi AB)$. As a reference, a cell of elliptical shape has D = 0; in our case, we expect low dispersion values for [NaCl] = 0. Application of this metric to our data (Fig. 5A, right) shows the expected behavior for no salt, and that the distributions are similar. A detailed look, however, reveals the development of a long tail for the distribution at high [Na] (noticeable in the cumulative distribution, inset of Fig. 5A, left). This behavior is consistent with the fact that plasmolysis induces void areas in the traditional shape of a bacterium, thereby departing from an approximately ellipsoid shape.

One characteristic of the distributions of area, elongation, dispersion, is that they are broad, regardless of salt condition. However, when plotting elongation vs. dispersion (Fig. 5B) we observe a narrow distribution at [NaCl] = 0. Moreover, the elongation vs. dispersion data at this no-salt condition follows an approximate linear relationship with a slope value ~20. This implies that small departures from an elliptical shape are accompanied by a drastic increase in elongation. This behavior occurs for cells at late stages of division, where the septum and the appearance of kinks in the overall elongated shape of the dividing cell contribute to an increase in dispersion. Finally, we note that the elongation vs. dispersion distribution broadens significantly with salt increase. Using this comparison, the distinction between regular and plasmolyzed cells is thus straightforward.

Altogether, we have shown that the methodology provided by the invariant moments to quantitatively characterize cell geometry is a simple, convenient, and accurate tool, with application for bacterial cells. Indeed, previous studies using this tool have focused

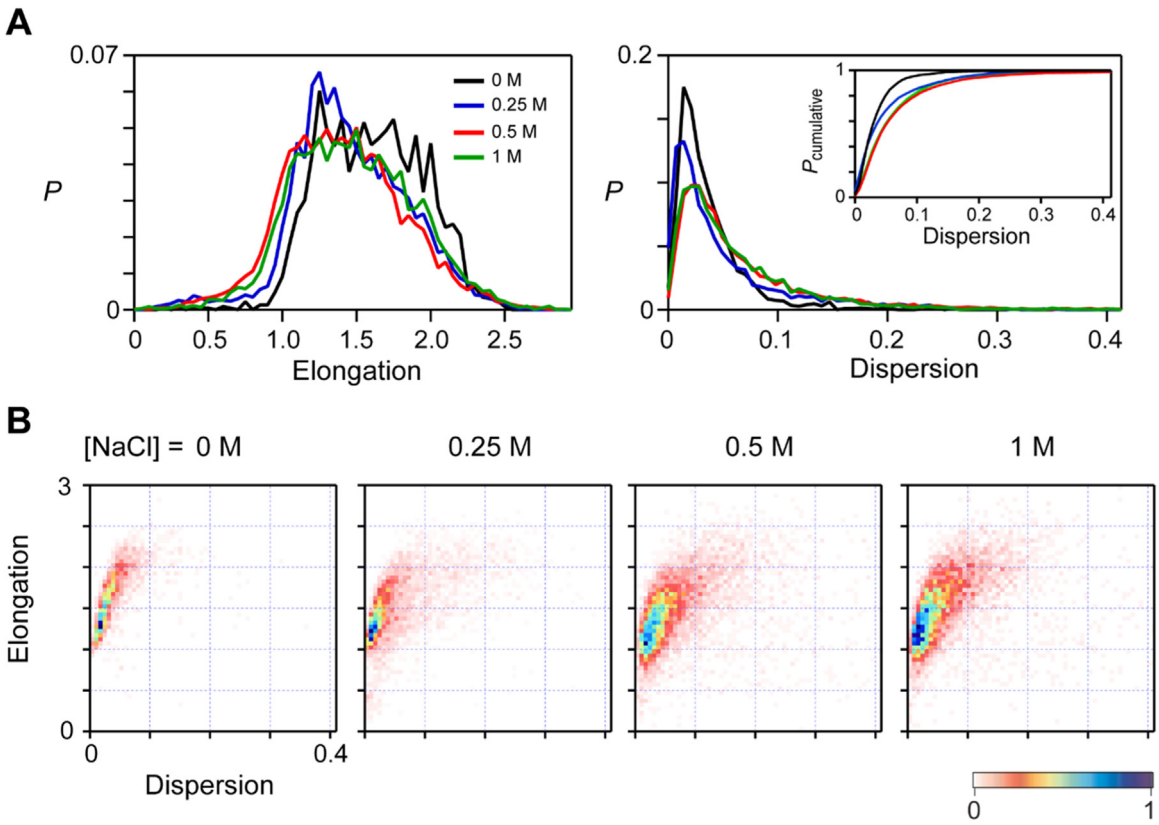

Fig. 5. Elongation and dispersion for bacterial cells subject to hyperosmotic shock. (A) The distributions for elongation. (B) The distributions for dispersion. Insets show the cumulative distributions. (c) 2D histograms of elongation vs. dispersion for all salt conditions tested.

on mammalian cells [20,21] or amoeba [22] to quantify motility or growth. With the application of increasing salt concentrations, we have shown that the invariant moments provide means to characterize the distinct *E. coli* populations (normal and plasmolyzed cells), using less involved and more robust computations compared with previously used methods for these cells [15].

Application of the invariant moments to bacterial plasmolysis has enabled us to estimate changes in area and volume upon increasing salt concentration. Moreover, we have found that cells reach a minimum volume (roughly half of the volume of the original cell) at [NaCl] = 0.5 M and increase in [NaCl] does not reduce the volume further, rather leading to events where full cell area is recovered (which we attribute to membrane rupture and filling of the capsule by the cytoplasm). The minimum volume found in plasmolyzed cells approaches the expected volume that is occupied by macromolecules in normal cells (20–30 %) [23], indicating a possibly factor involved in establishing said minimum volume. Lastly, in highly plasmolyzed cells elongation is much reduced, posing challenges to algorithms that measure size based on “caliper” methods (as they must characterize cells along multiple directions). By computing global metrics, the method of invariant moments does not suffer from this problem, providing an excellent alternative for the characterization of geometry in cells.

Limitations

Not applicable.

Ethics statements

None.

CRediT author statement

Braulio Gutiérrez-Medina. Conceptualization, Methodology, Software, Formal Analysis, Data curation, Writing- Original draft preparation, Visualization, Supervision, Writing- Reviewing and Editing, Funding acquisition.

Declaration of competing interest

The authors declare that they have no known competing financial interests or personal relationships that could have appeared to influence the work reported in this paper.

Data availability

Data will be made available on request.

Acknowledgments

This work was supported by CONAHCYT (Mexico) grant CF-2023-G-542 to B.G.-M.

References

[1] K. Keren, et al., Mechanism of shape determination in motile cells, Nature 453 (7194) (2008) 475–480, doi:10.1038/nature06952.
[2] A. Mogilner, K. Keren, The shape of motile cells, Curr. Biol. 19 (17) (2009) R762–R771.
[3] E. Paluch, C.-P. Heisenberg, Biology and physics of cell shape changes in development, Curr. Biol. 19 (17) (2009) R790–R799, doi:10.1016/j.cub.2009.07.029.
[4] A.F.M. Marée, V.A. Grieneisen, L. Edelstein-Keshet, How cells integrate complex stimuli: the effect of feedback from phosphoinositides and cell shape on cell polarization and motility, PLoS. Comput. Biol. 8 (3) (2012) e1002402 -Mar.[Online]Available, doi:10.1371/journal.pcbi.1002402.
[5] T.M. Maul, D.W. Chew, A. Nieponice, D.A. Vorp, Mechanical stimuli differentially control stem cell behavior: morphology, proliferation, and differentiation, Biomech. Model. Mechanobiol. 10 (6) (2011) 939–953, doi:10.1007/s10237-010-0285-8.
[6] H. Jeckel, K. Drescher, Advances and opportunities in image analysis of bacterial cells and communities, FEMS Microbiol. Rev. 45 (4) (2021) fuaa062 Jul., doi:10.1093/femsre/fuaa062.
[7] T. Tang, et al., Microscopic impedance cytometry for quantifying single cell shape, Biosens. Bioelectron. 193 (Dec. 2021) 113521, doi:10.1016/j.bios.2021.113521.
[8] T. Vicar, et al., Cell segmentation methods for label-free contrast microscopy: review and comprehensive comparison, BMC. Bioinformat. 20 (1) (2019) 360, doi:10.1186/s12859-019-2880-8.
[9] A.E. Carpenter, et al., CellProfiler: image analysis software for identifying and quantifying cell phenotypes, Genome Biol. 7 (10) (2006) R100, doi:10.1186/gb-2006-7-10-r100.
[10] E. Alizadeh, W. Xu, J. Castle, J. Foss, A. Prasad, TISMorph: a tool to quantify texture, irregularity and spreading of single cells, PLoS. One 14 (6) (2019) e0217346 -Jun.[Online]Available, doi:10.1371/journal.pone.0217346.
[11] P. Barbier de Reuille, et al., MorphoGraphX: a platform for quantifying morphogenesis in 4D, Elife 4 (2015) e05864, doi:10.7554/eLife.05864.
[12] P.B. de Reuille, S. Robinson, R.S. Smith, Quantifying cell shape and gene expression in the shoot apical meristem using MorphoGraphX, in: V. Žárský, F. Cvrčková (Eds.), Plant Cell Morphogenesis: Methods and Protocols, Humana Press, Totowa, NJ, 2014, pp. 121–134, doi:10.1007/978-1-62703-643-6_10.
[13] L.G. Alexopoulos, G.R. Erickson, F. Guilak, A method for quantifying cell size from differential interference contrast images: validation and application to osmotically stressed chondrocytes, J. Microsc. 205 (2) (2002) 125–135 Feb., doi:10.1046/j.0022-2720.2001.00976.x.
[14] C. Kempster, et al., Fully automated platelet differential interference contrast image analysis via deep learning, Sci. Rep. 12 (1) (2022) 4614, doi:10.1038/s41598-022-08613-2.
[15] B. Gutiérrez-Medina, M. de J. Sánchez Miranda, Quantitative image restoration in bright field optical microscopy, Biophys. J. 113 (9) (2017) 1916–1919 Nov., doi:10.1016/j.bpj.2017.09.002.
[16] B. Möller, Y. Poeschl, R. Plötner, K. Bürstenbinder, PaCeQuant: a tool for high-throughput quantification of pavement cell shape characteristics, Plant Physiol. 175 (3) (2017) 998–1017 Nov., doi:10.1104/pp.17.00961.
[17] 16–19 G.A. Dunn, A.F. Brown, Quantifying cellular shape using moment invariants, in: W. Alt, G. Hoffmann (Eds.), Biological Motion: Proceedings of a Workshop held in Königswinter, Germany, March, Springer Berlin Heidelberg, Berlin, Heidelberg, 1989, pp. 10–34, doi:10.1007/978-3-642-51664-1_2. 16–191990.
[18] D. Sage, et al., DeconvolutionLab2: an open-source software for deconvolution microscopy, Methods 115 (Feb. 2017) 28–41, doi:10.1016/j.ymeth.2016.12.015.
[19] M.R. Teague, Image analysis via the general theory of moments, J. Opt. Soc. Am. 70 (8) (Aug. 1980) 920, doi:10.1364/JOSA.70.000920.
[20] P. Dieterich, J. Seebach, and H.-J. Schnittler, "Quantification of shear stress-induced cell migration in endothelial cultures," in function and regulation of cellular systems, A. Deutsch, J. Howard, M. Falcke, and W. Zimmermann, Eds., Basel: Birkhäuser Basel, 2004, pp. 199–207. doi: 10.1007/978-3-0348-7895-1_18.
[21] D. Zicha, G.A. Dunn, An image processing system for cell behaviour studies in subconfluent cultures, J. Microsc. 179 (1) (1995) 11–21 Jul., doi:10.1111/j.1365-2818.1995.tb03609.x.
[22] D. Dormann, T. Libotte, C.J. Weijer, T. Bretschneider, Simultaneous quantification of cell motility and protein-membrane-association using active contours, Cell Motil. 52 (4) (2002) 221–230 Aug., doi:10.1002/cm.10048.
[23] R.J. Ellis, Macromolecular crowding: an important but neglected aspect of the intracellular environment, Curr. Opin. Struct. Biol. 11 (1) (2001) 114–119 Feb., doi:10.1016/S0959-440X(00)00172-X.